A Low Voltage AC Input Boost Fly Back Converter as a High Power Factor Off-Line Power Supply

SRAVAN KUMAR S. L. V.[1], RAVISANKARA REDDY N.[2], VIJAYA KUMAR M.[3], RAGHAVAIAH KATURI[4]

[1]Department of EEE, JNTUA,
Anantapur, Andhra Pradesh,
INDIA

[2]Department of EEE, G. Pulla Reddy Engineering College,
Kurnool, Andhra Pradesh,
INDIA

[3]Department of EEE, JNTUA,
Anantapur, Andhra Pradesh,
INDIA

[4]Department of EEE, VFSTR Deemed to be University,
Guntur, Andhra Pradesh,
INDIA

Abstract: - In this paper a boost fly back converter with series and parallel configuration is introduced. This topology is a better way to implement low-cost high-power factor ac-dc converters with better output voltage regulation. The main advantages of this topology are a single switch is sufficient for both boost and fly back operations, voltage across the Power MOSFET is less and no requirement of snubber circuits. The fly back transformer is chosen as 1:1 transformer because of less stray inductance and low leakage inductance loss. The midpoint configuration type high frequency fly back transformer is used at primary side to obtain series and parallel combination of bulk capacitors and primary windings transformer. An input voltage of 28V AC 48V output DC 48W operating at 100Khz switching frequency AC to DC converter is presented. Hysteresis Current Control technique is used to control the switch and MATLAB Simulink is used to obtain the simulation results and FPGA SPARTRAN 6 is used to generate PWM signals for Hardware Implementation.

Key-Words: - Boost converter, fly back converter, Hysteresis Current Control, MATLAB, FPGA SPARTRAN 6, MOSFET, DC-DC Converter, Integrated Isolated DC-DC Converter.

Received: March 21, 2025. Revised: August 9, 2025. Accepted: August 26, 2025. Published: December 31, 2025.

1 Introduction

In present days, renewable sources like wind and solar usage have been rapidly increased through the world. With these energy sources greenhouse emissions are not released into the environment. Ten years back i.e. 2011 due to severe earthquake Japan country was majorly affected. Due to damage of several reactors in Fukushima nuclear plant a higher amount of radioactive element spreads into the atmosphere which is nothing but increasing of greenhouse emissions. This situation in Japan demands complete shutdown of nuclear power plant and also public in Japan already have awareness of green energy. Therefore, to reduce pollution, fossil fuels and safety issues development of green energy is the best alternative to generate electricity. Along with solar and wind fuel cells are also used as auxiliary energy source in some applications like Electric Vehicles, emergency backup power and portable electronics etc., [1], [2], [3], [4], [5]. In some applications low voltage input and medium or high voltage output voltage is required. Hence a boost configuration-based topologies need to implement for different applications.

The high voltage output can be obtained using non isolated and isolated converters. The main advantage of isolated converters is energy storage, provides isolation and no output filter inductor is required in case of fly back converter. Where as in case of full bridge, half bridge and push pull converters a output filter inductor is used. The output voltage can be increased by varying the turns ratio of the transformer, [6], [7], [8], [9], [10].

But the main disadvantage is leakage inductance is increases which reduces the converter efficiency and also increases the switching stress, [11], [12], [13], [14], [15]. To decrease the voltage spike across the MOSFET again snubber circuits are used. For the fly back topology generally two snubber circuits are required one is across transformer and another one is across MOSFET switch. Generally conventional non isolated converter Boost, Buck – Boost can achieve high voltage gain. Non-isolated topologies with high output gain have been discussed in past decade, [16], [17], [18], [19], [20]. These non-isolated converters can be developed with the help of coupled inductors, cascaded techniques, switched capacitors techniques. But there is no isolation in these converters which are not meeting the required safety standards. To achieve galvanic isolation isolated converters are preferred. In this paper fly back topology is considered because the power limitation is below 100W.

Figure 1 shows small wind power generation for low power and high voltage gain applications with low voltage input.

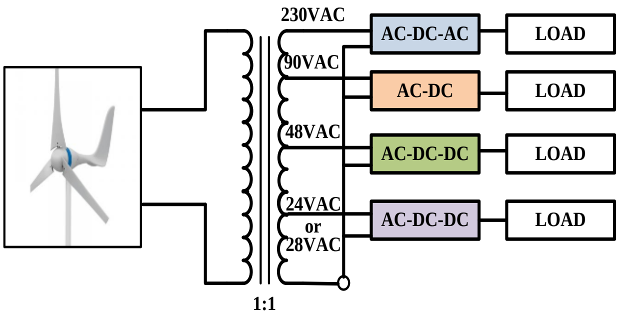

Fig. 1: Structure of Wind for Low Power Loads

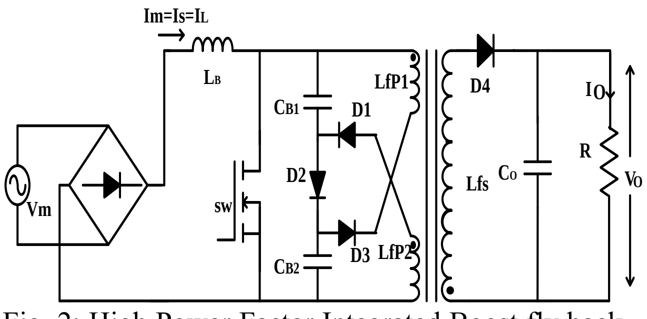

Fig. 2: High Power Factor Integrated Boost fly back converter with Series and Parallel Combination

The wind power can generate up to 230V or 440V. For some applications the input voltage requirement is 230VAC or 90VAC or 48VAC or 28V AC, therefore an isolation transformer with tapings is used to supply the power to converters.

In this paper operation and mathematical analysis of single stage integrated boost fly back converter is discussed. Section 2 presents the operating modes of AC-DC single stage integrated boost fly back converter along with the waveforms. Section 3 presents the calculation of design parameters for the proposed converter. Section 4 presents simulation results and section 5 hardware results of the converter. In the last, conclusions are provided in section 6.

2 Operation of Single Stage Boost Fly Back Converter

The circuit diagram of boost fly back converter in series parallel combination as shown in Figure 2. The different modes of operation of proposed converter as shown in Figure 3 and the few waveforms related to the operating modes shown in Figure 4.

Mode 1[0< t< t1: Figure 3(a)]: When the supply voltage Vm and VLB is greater than VCB1 +VCB2 the diode bridge rectifier is turned on and the voltage developed after the bridge rectifier is Vdc. Assume initially capacitors CB1 and CB2 are charged. When the MOSFET SW is ON three currents will flows through the MOSFET SW. The first current path from AC source is Vm-Bridge rectifier- LB-SW-(-Vm). The current paths from the Capacitors CB1, CB2 are CB1-SW-Lfp2-D1-CB1 and CB2-D3-Lfp1-SW-CB2 are shown in Figure 3(a). In this mode of operation, the current through boost inductor LB is slowly increases and due to the opposite polarity of primary and secondary transformer the diode D4 is forward biased and the power will transfer to the load. In this mode of operation diode D2 is turned off due to the capacitors discharging and diode D2 will turn ON when it is charging. The corresponding equations are:

$$-V_{DC} + V_{LB} = 0 \quad (1)$$

$$V_{DC} = V_{LB} \quad (2)$$

Where $V_{DC} = \frac{2V_m}{\pi}$.

Also

$$-V_{CB1} + V_{LFP2} = 0$$

$$V_{CB1} = V_{LFP2} \quad (3)$$

Similarly,

$$V_{CB2} = V_{LFP1} \quad (4)$$

$$V_{LFS} = V_{LFP1} + V_{LFP2} = V_o \quad (5)$$

Mode 2[t1< t< t2: Figure 3(b)]: In this mode of operation also the supply voltage Vm and VLB is greater than VCB1+VCB2. But in this case the MOSFET SW is off the stored energy in the inductor LB is delivering to the capacitors, then the first current path is +Vm- bridge Rectifier-LB-CB1-D2-CB2-(-Vm). Similarly, the energy stored in the primary windings of the transformers delivering its energy to the capacitors CB1 and CB2. Therefore, the other two current paths are +Lfp1-CB1-D2- D3-(-Lfp1) and +Lfp2- D1-D2- CB1 (-Lfp1) are shown in Figure 3(b). Due to the opposite polarity of the primary and secondary side of transformer diode D4 is reverse bias and output capacitor Co discharges its energy to the load. The corresponding equations are:

$$-V_{DC} - V_{LB} + V_{SW} = 0 \quad (6)$$

$$V_{SW} = V_{DC} + V_{LB} \quad (7)$$

The voltage across the switch equation can also be written as:

$$V_{SW} = V_{CB1} + V_{CB2} = V_{CB} \quad (8)$$

Mode 3[t2< t< t3: Figure 3(c)]: In this mode of operation the supply voltage Vm and VLB is less than VCB1+VCB2 due to this the diode bridge rectifier is reverse bias and the current flows from the source is zero. In this mode of only fly back operation is performed and the bulk capacitors CB1 and CB2 discharges its energy to the primary winding of fly back transformers. When the switch is on then the current flows through CB1-SW-Lfp2-D1-CB1 and CB2-D3-Lfp1-SW-CB2 are shown in Figure 3(c). Here the diode D2 is turned off and also D4 is ON due to opposite polarity of the primary winding of the transformer.

Mode 4[t3< t< t4: Figure 3(d)]: In this mode of operation the supply voltage Vm and VLB is less than VCB1+VCB2 due to this the diode bridge rectifier is reverse bias and the no current flows from the source. In this mode the Mosfet SW is turned off and current paths are +Lfp1-CB1-D2-D3-(-Lfp1) and +Lfp2-D1-D2-CB2-(-Lfp2) are shown in Figure 3(d). In this mode D2 is ON but D4 is OFF and capacitor Co is supplying power to the load. In other words, here fly back transformer gives energy to the Bulk capacitors CB1 and CB2. The bridge rectifier and Input current waveform as shown in Figure 5.

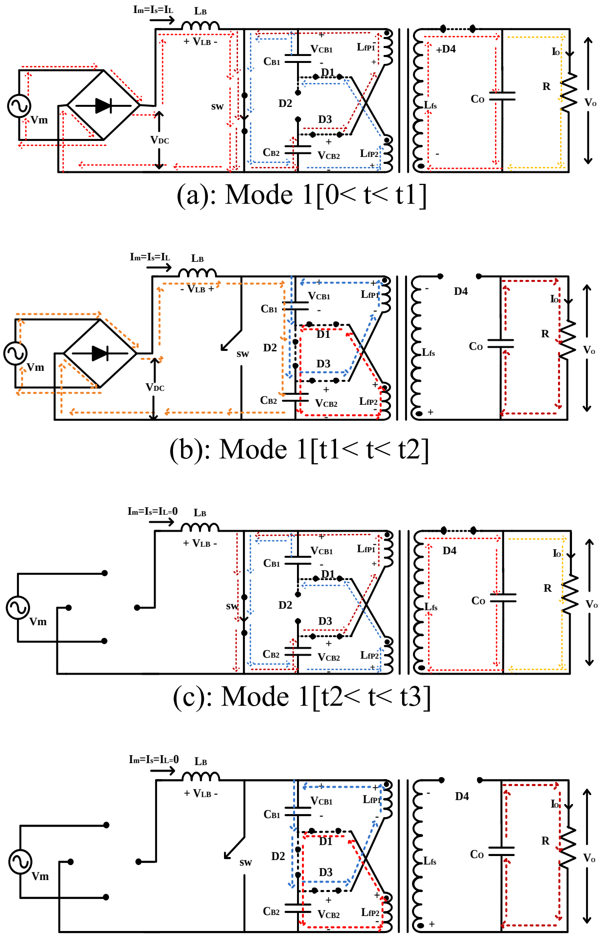

(a): Mode 1[0< t< t1]

(b): Mode 1[t1< t< t2]

(c): Mode 1[t2< t< t3]

(d): Mode 1[t3< t< t4]

Fig. 3: Modes of Boost fly back converter with series and parallel combination

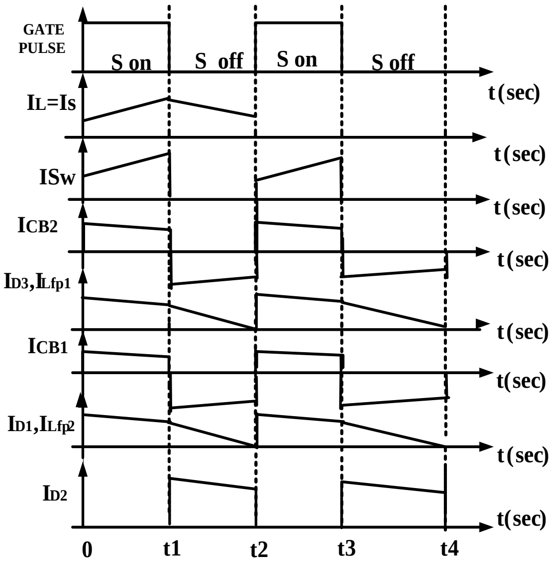

Fig. 4: Switching Waveforms of Proposed Converter

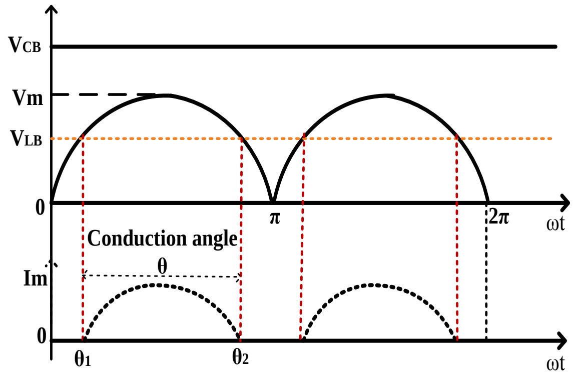

Fig. 5: Bridge Rectifier and Input current waveforms Without EMI filter

From the waveforms it is observed that if Vm+VLB is greater than VCB1+VCB2=VCB the source current Im=Is=IL is present and when Vm+VLB is less than VCB1+VCB2=VCB the source current is absent.

The conduction angle θ can be calculated as:

$$V_m sin\omega t + V_{LB} = V_{CB} \tag{9}$$

$$\omega t = \sin^{-1}\frac{(V_{CB}-V_{LB})}{V_m} = \theta 1 \tag{10}$$

$$\theta 2 = \pi - \theta 1 \tag{11}$$

Conduction angle $\theta = \theta 2 - \theta 1$ (12)

In case of EMI Filter added at source side the source inductance will be considered while calculating the conduction angle. The Figure 6 shows the Bridge rectifier and Input current waveforms when EMI Filter is added at source side:

$$\omega t = \sin^{-1}\frac{(V_{CB}-V_{LS}-V_{LB})}{V_m} = \theta 1 \tag{13}$$

To find the $\theta 2$ and conduction angle Eq. 11 and Eq.12 are used.

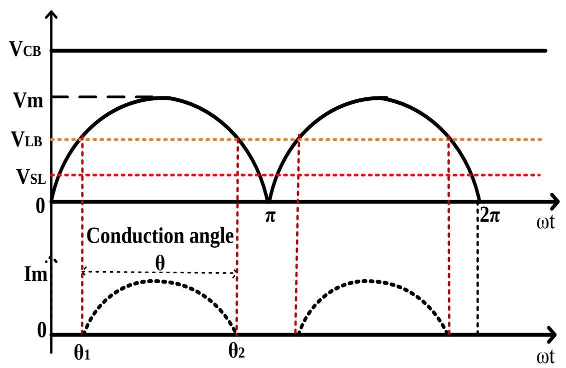

Fig. 6: Bridge Rectifier and Input current waveforms with EMI filter

Here VSL is nothing but voltage of source inductance.

$$V_m sin\omega t + V_{LB} + V_{LS} = V_{CB} \tag{14}$$

3 Design Example

The design specifications are considered as source voltage in terms of RMS =27V and Vm= 38V, Vo=48V, Io=1A, Po=48W, Duty cycle D=50%, Switching frequency fs=100Khz, $\Delta I = 0.25A$

From Eq.2 The bridge rectifier output Voltage can be calculated as:

$$V_{DC} = \frac{2V_m}{\pi}. = \frac{2*38}{3.14} = 24V = V_{LB} \tag{15}$$

From Eq.7 $V_{SW} = V_{DC} + V_{LB}$

$$V_{SW} = 24 + 24 = 48V \tag{16}$$

From the equation (8)

$V_{SW} = V_{CB1} + V_{CB2} = V_{CB}$

There fore $V_{CB1} = V_{CB2} = 24V$ (17)

From Eq.3 and Eq.4 $V_{CB1} = V_{LFP2}$

$$V_{LFP2} = 24V \tag{18}$$

Similarly, $V_{LFP1} = 24V$ (19)

From the Eq.5$V_{LFS} = V_{LFP1} + V_{LFP2} = V_o$

$$V_{LFS} = 24 + 24 = 48 = V_o \tag{20}$$

The output Voltage Vo can also have calculated from the basic output voltage equation as follows:

$$V_o = \frac{V_{DC}}{1-D} \tag{21}$$

$$V_o = \frac{V_{DC}}{1-D} = \frac{24}{1-0.5} = 48V \tag{22}$$

The boost inductance LB can be calculated as:

$$L_B = \frac{V_{CB}*D}{f_s*\Delta i} \tag{23}$$

$$L_B = \frac{48*0.5}{100000*0.25} = 1mH \tag{24}$$

The boost capacitance can be calculated as:

$$C_{B1} = C_{B2} = \frac{D*Io}{f_s*\Delta Vc} \tag{25}$$

$$C_{B1} = C_{B2} = \frac{0.5*1}{100000*0.01} = 500\mu F \tag{26}$$

The fly back inductance can be calculated as:

$$P = \frac{V_{CB*}^2 D^2}{2*L_{fp}*f_s} \tag{27}$$

$$48 = \frac{48_*^2 0.5^2}{2*L_{fp}*100000}$$

$$L_{fp} = 60\mu H \tag{28}$$

The source current can be calculated as:

$$I_s = \frac{I_o}{1-D} \tag{29}$$

$$I_s = \frac{1}{1-0.5} = 2A \tag{30}$$

The conduction angle θ can be calculated for the proposed converter without EMI filter as follows:
From Eq. 10 $\theta 1$ can be calculated as:

$$\omega t = \sin^{-1}\frac{(48-24)}{38} = 39.16° = \theta 1 \tag{31}$$

From Eq.11 $\theta 2 = \pi - \theta 1$

$$\theta 2 = \pi - 39.16° = 140.84° \tag{32}$$

From Eq.12 $\theta = \theta 2 - \theta 1$
Conduction angle

$$\theta = 140.84 - 39.16 = 101.68° \tag{33}$$

The conduction angle θ can be calculated for the proposed converter with EMI filter as follows:
From Eq. 14 $\theta 1$ can be calculated as:

$$\omega t = \sin^{-1}\frac{(V_{CB} - V_{LS} - V_{LB})}{V_m} = \theta 1$$

$$V_{LS} = I * X_{LS} \tag{34}$$

$$V_{LS} = I * 2 * 3.14 * f * L_S$$
$$V_{LS} = 2 * 2 * 3.14 * 50 * 1e - 3 = 0.628V \tag{35}$$

$$\omega t = \sin^{-1}\frac{(48-0.628-24)}{38} = 37.8° = \theta 1 \tag{36}$$

$$\theta 2 = \pi - 37.8° = 142.2° \tag{37}$$

Conduction angle

$$\theta = 142.2 - 37.8 = 104.4° \tag{38}$$

4 Simulation Results of AC/DC Converter without EMI Filter

Figure 7 shows output voltage of AC/DC Converter and magnitude is 46.13V, Figure 8 shows output current of AC/DC Converter and the magnitude is 0.965A. Figure 9 shows Capacitor voltage of AC/DC Converter and the minimum voltage is 25V and maximum Voltage is 35V. Figure 10 shows transformer primary Voltage Lfp1 and the positive voltage magnitude is 26V and negative voltage magnitude is 23V. Figure 11 shows transformer secondary voltage Lfs and the positive voltage magnitude is 50V and negative voltage magnitude is 46V. Figure 12 switch voltage of Ac/DC Converter and the magnitude is 50V. Figure 13 Input VA of Ac/DC converter, Figure 14 capacitor current of Ac/DC Converter, Figure 15 shows FFT analysis of AC/DC Converter with peak value of current is 4.216A and RMS value is 2.9A.

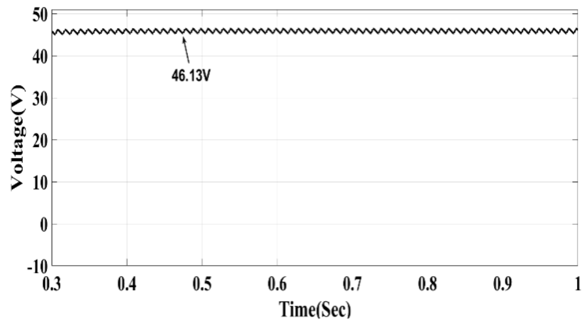

Fig. 7: Output Voltage of AC/DC Converter without EMI Filter

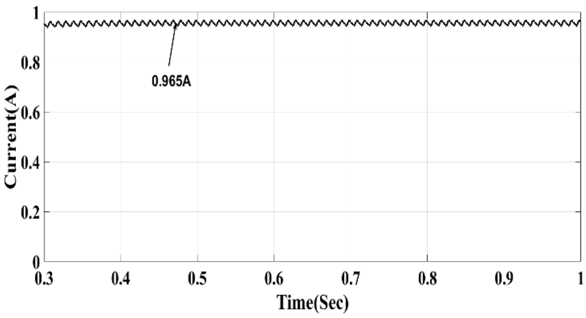

Fig. 8: Output Current of AC/DC Converter without EMI Filter

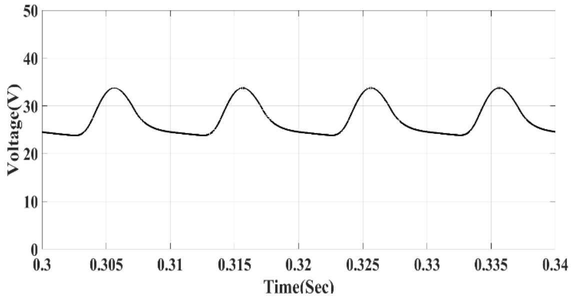

Fig. 9: Capacitor Voltage CB1 of AC/DC Converter without EMI Filter

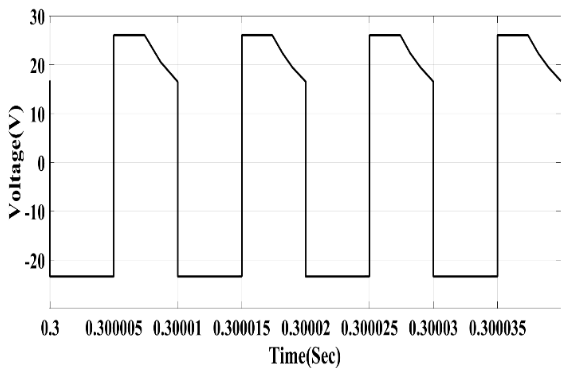

Fig. 10: Transformer Primary Voltage Lfp1 of AC/DC Converter without EMI Filter

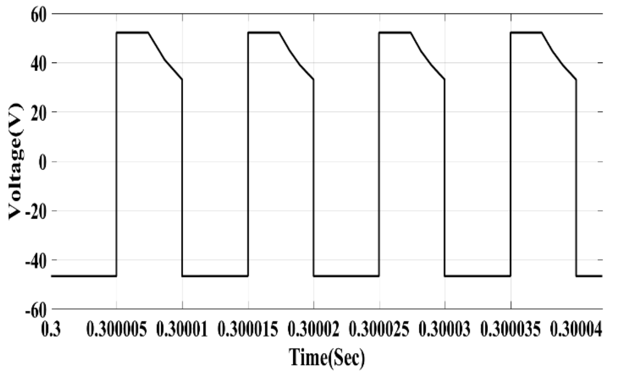

Fig. 11: Transformer Secondary Voltage Lfs of AC/DC Converter without EMI Filter

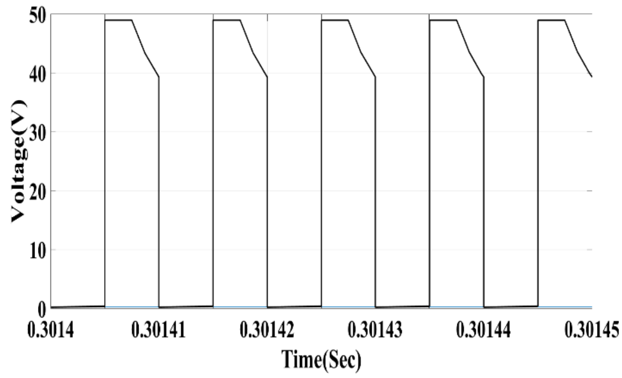

Fig. 12: Switch Voltage of Ac/DC Converter without EMI Filter

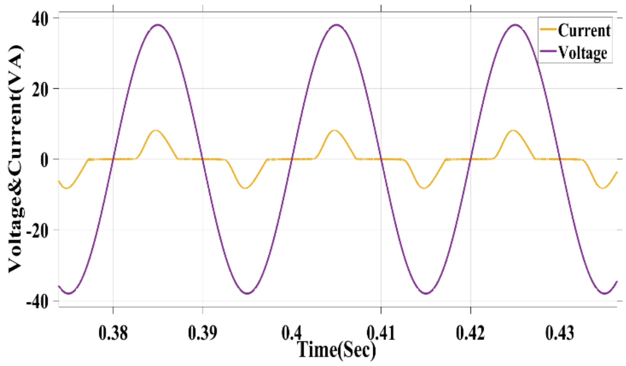

Fig. 13: Input VA of Ac/DC Converter without EMI Filter

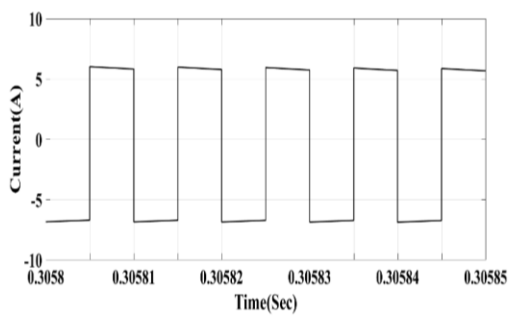

Fig. 14: Capacitor Current of Ac/DC Converter without EMI Filter

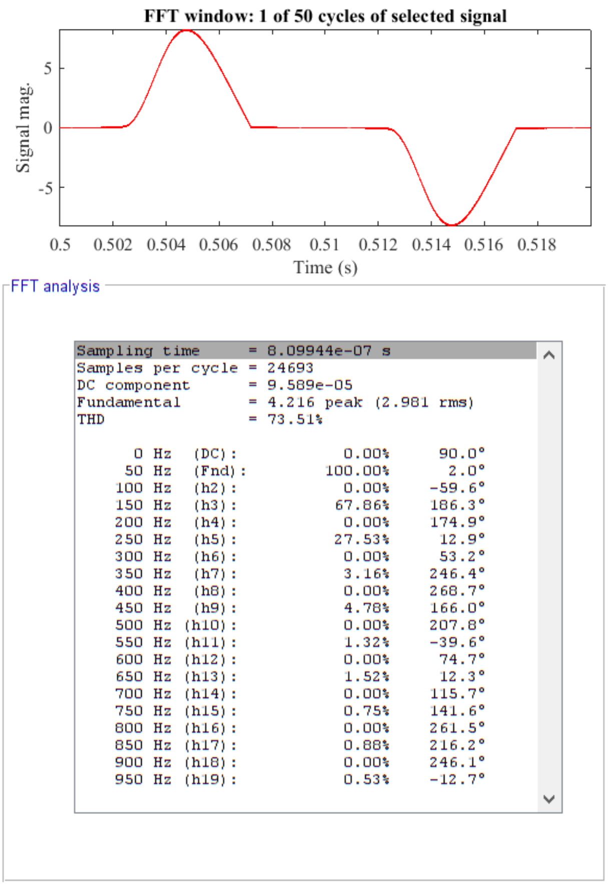

Fig. 15: FFT Analysis of Ac/DC Converter without EMI Filter

From the Figure 13 the Displacement Power Factor (DPF) can be identified as 0.99 and THD form Figure 15 can be identified as 73.51. The Power Factor can be calculated as:

$$PF = \frac{DPF}{\sqrt{1+THD^2}} \tag{39}$$

$$PF = \frac{0.99}{\sqrt{1+0.73^2}} = 0.8 \tag{40}$$

from the Figure 15 and from Eq.12 conduction angle

$$\theta = (0.5072 - 0.5021) * \frac{180}{0.01} = 92° \tag{41}$$

4.1 Simulation Results of AC/DC Converter with EMI Filter

Figure 16 shows output voltage of AC/DC Converter and magnitude is 46.12V, Figure 17 shows output current of AC/DC Converter and the magnitude is 0.96A. Figure 18 shows Capacitor voltage of AC/DC Converter and the minimum voltage is 25V and maximum Voltage is 35V. Figure 19 shows transformer primary Voltage Lfp1 and the positive voltage magnitude is 26V and negative voltage magnitude is 23V. Figure 20 shows transformer secondary voltage Lfs and the positive voltage magnitude is 50V and negative voltage magnitude is 46V. Figure 21 switch voltage of Ac/DC Converter and the magnitude is 58V, Figure 22 capacitor current of Ac/DC Converter, Figure 23 Input VA of Ac/DC converter, Figure 24 shows FFT analysis of AC/DC Converter with peak value of current is 4.142A, RMS value is 2.929A and THD is 61.20%.

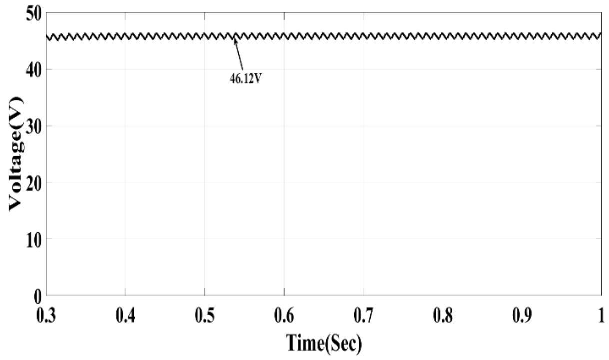

Fig. 16: Output Voltage of AC/DC Converter with EMI Filter

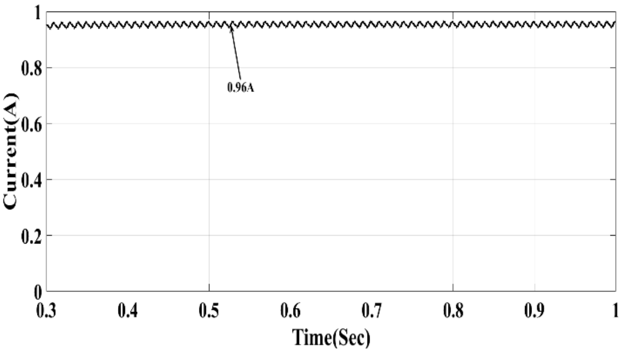

Fig. 17: Output Current of AC/DC Converter without EMI Filter

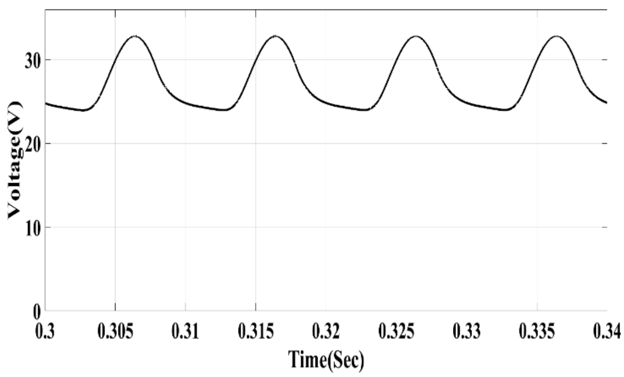

Fig. 18: Capacitor Voltage CB1 of AC/DC Converter without EMI Filter

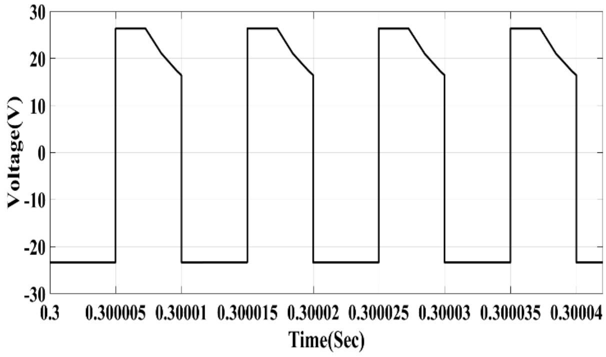

Fig. 19: Transformer Primary Voltage Lfp1 of AC/DC Converter with EMI Filter

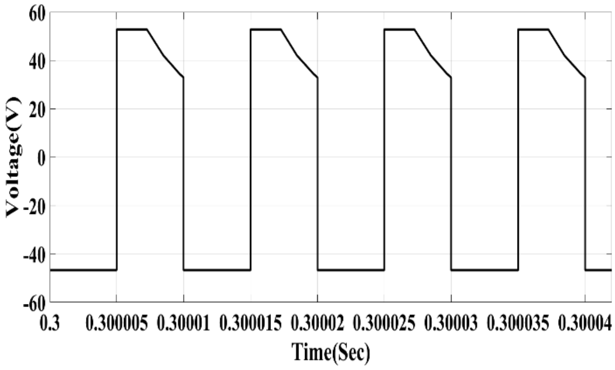

Fig. 20: Transformer Secondary Voltage Lfs of AC/DC Converter with EMI Filter

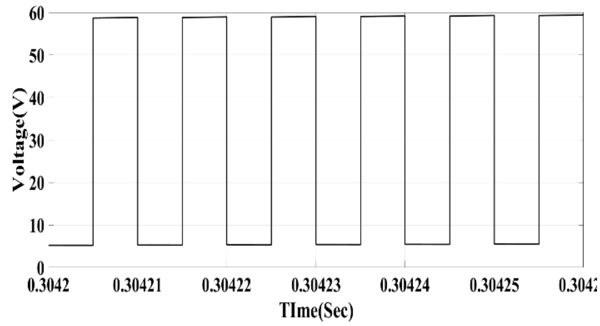

Fig. 21: Switch Voltage of Ac/DC Converter with EMI Filter

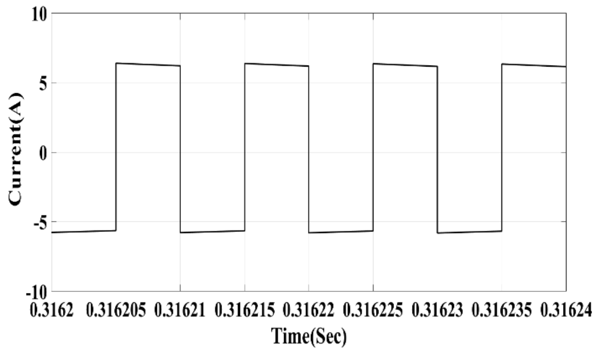

Fig. 22: Capacitor Current of Ac/DC Converter with EMI Filter

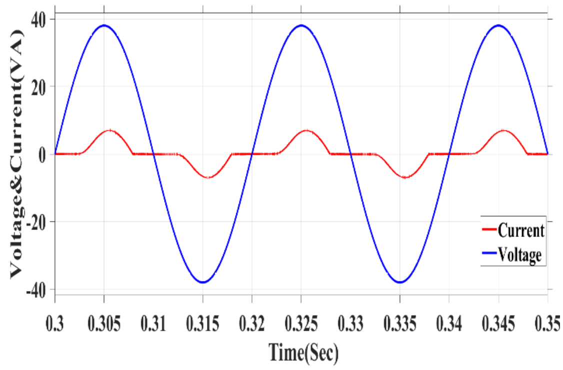

Fig. 23: Input VA of Ac/DC Converter with EMI Filter

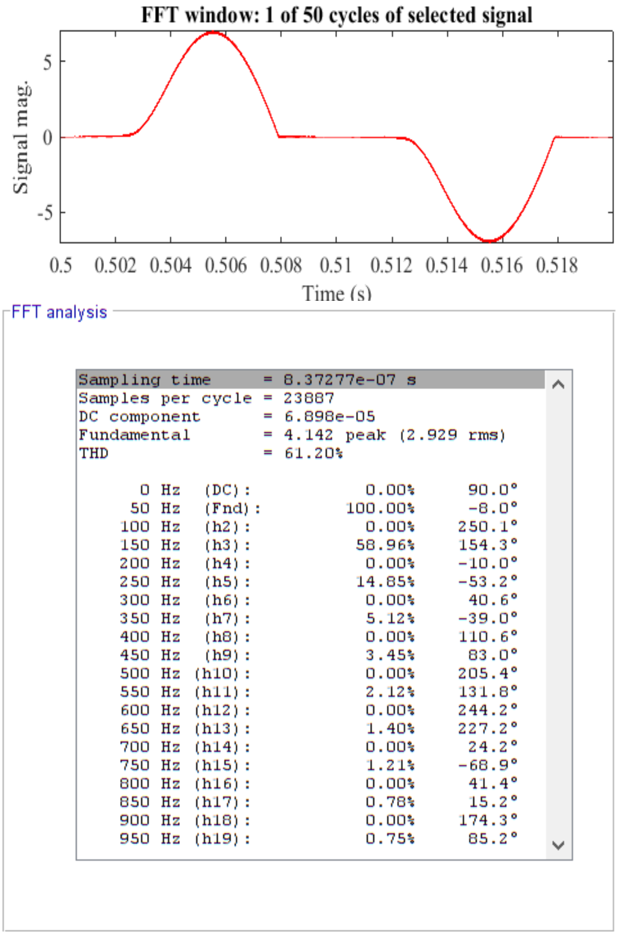

Fig. 24: FFT Analysis of Ac/DC Converter without EMI Filter

From the Figure 23 the Displacement Power Factor (DPF) can be identified as 0.99 and THD form Figure 15 can be identified as 73.51. The Power Factor can be calculated as:

$$PF = \frac{DPF}{\sqrt{1+THD^2}} \tag{42}$$

$$PF = \frac{0.99}{\sqrt{1+0.612^2}} = 0.84 \tag{43}$$

from the Figure 15 and from Eq.12 conduction angle

$$\theta = (0.5079 - 0.5021) * \frac{180}{0.01} = 104.4° \tag{44}$$

From the above two topologies it is observed that the output voltage is without EMI Filter 46.13V and with EMI filter 46.12V. Also, the power factor and THD without EMI filter is 0.8 and 73.51%, With EMI Filter is 0.84 and 61.2%. To get the required output voltage and better power factor and THD a hysteresis current control is preferred.

4.2 Simulation Results of AC/DC Converter using Hysteresis current control

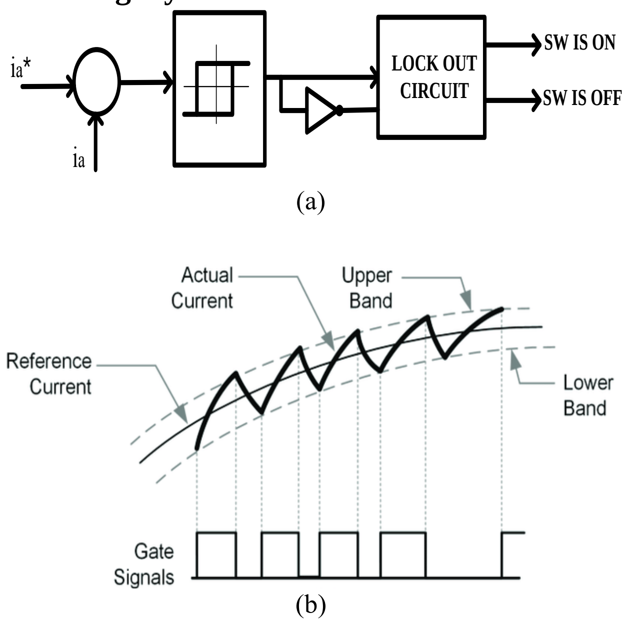

Fig. 25: (a) Hysteresis current control Block diagram, (b) waveform representation

In this hysteresis current controller ia* is nothing but reference current generator and it is generated with the help of bridge rectifier output voltage multiplied with PID controller. The current ia is nothing but inductor current which is given to hysteresis band to generate the PWM Pulses.

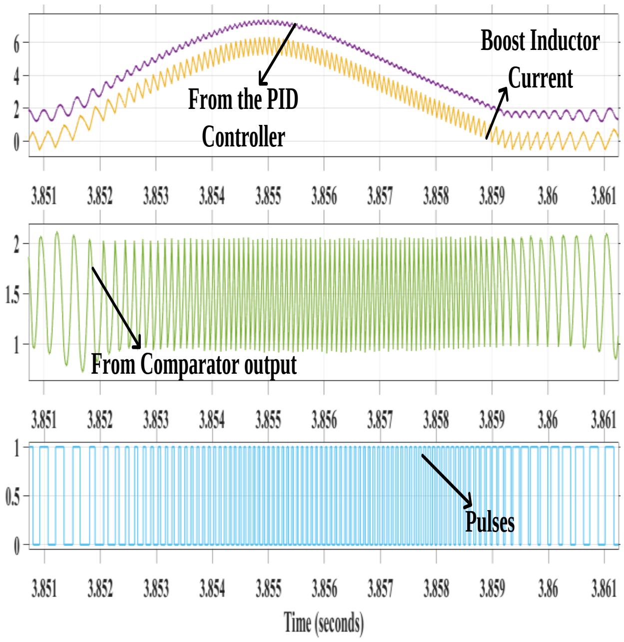

Fig. 26: Hysteresis Current Control Pulse Pattern

It is observed that from Figure 26 frequency of the pulses is varies because the reference current and sensing current variation. In the mat lab simulation for the hysteresis band switch on point is considered as 2 and switch off point is considered as 1.

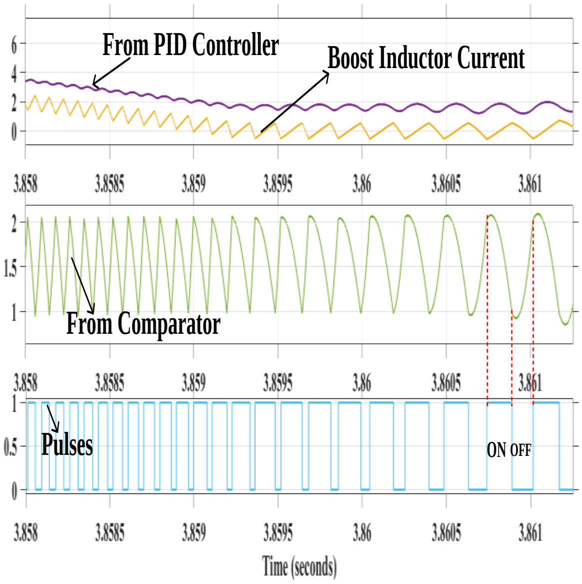

Fig. 27: Zoomed view of Hysteresis Current Control Pulse Pattern

From Figure 27 the ON pulse is presented when the comparator output is changing from 2 to 1 and OFF Pulse is presented when the comparator output is changing from 1 to 2.

Figure 28 shows output voltage of AC/DC Converter and magnitude is 48V, Figure 29 shows output current of AC/DC Converter and the magnitude is 1A. Figure 30 shows Capacitor voltage of AC/DC Converter and the minimum voltage is 7V and maximum Voltage is 26V. Figure 31 shows transformer primary Voltage Lfp1 and the positive voltage magnitude is 23V and negative voltage magnitude is 27V. Figure 32 shows transformer secondary voltage Lfs and the positive voltage magnitude is 48V and negative voltage magnitude is 48V. Figure 33 switch voltage of Ac/DC Converter and the magnitude is 51V. Figure 34 Input VA of Ac/DC converter, Figure 35 shows FFT analysis of AC/DC Converter with peak value of current is 4.711A, RMS value is 3.33A and THD is 24.87%.

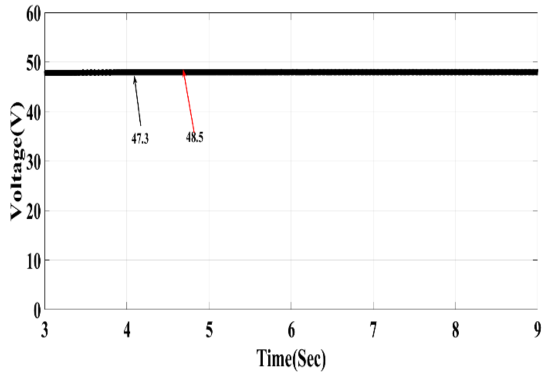

Fig. 28: Output Voltage using Hysteresis Current Control

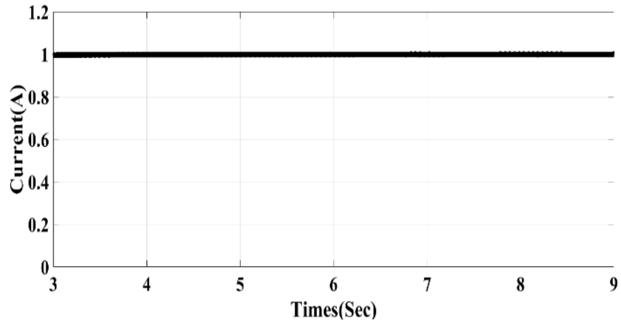

Fig. 29: Output Current using Hysteresis Current Control

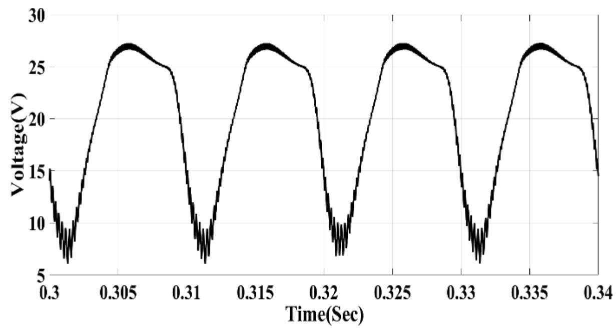

Fig. 30: Capacitor Voltage using Hysteresis Current Control

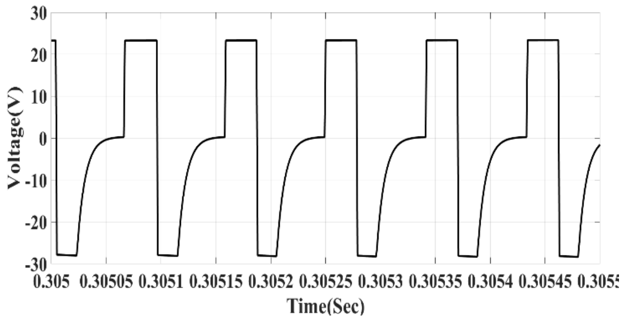

Fig. 31: Transformer Primary Lfp1 Voltage using Hysteresis Current Control

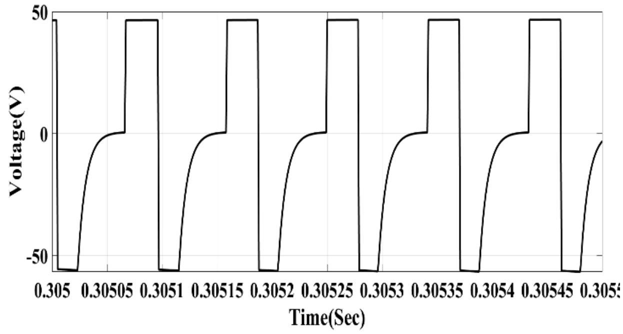

Fig. 32: Transformer secondary Lfs Voltage using Hysteresis Current Control

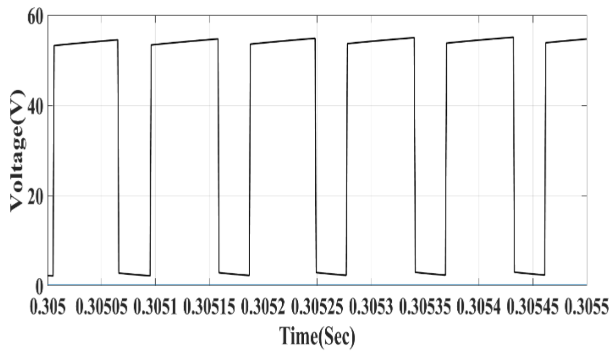

Fig. 33: Switch Voltage using Hysteresis Current Control

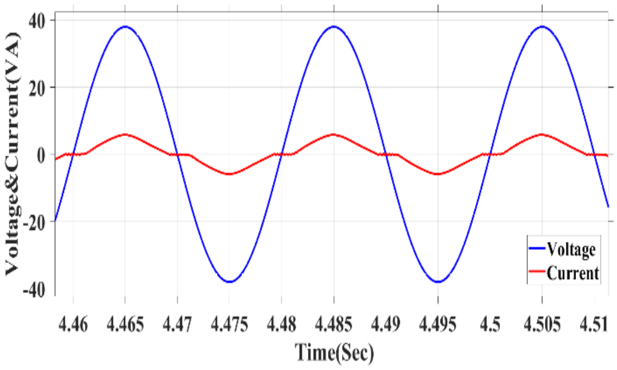

Fig. 34: Input VA of Ac/DC Converter using Hysteresis current Control

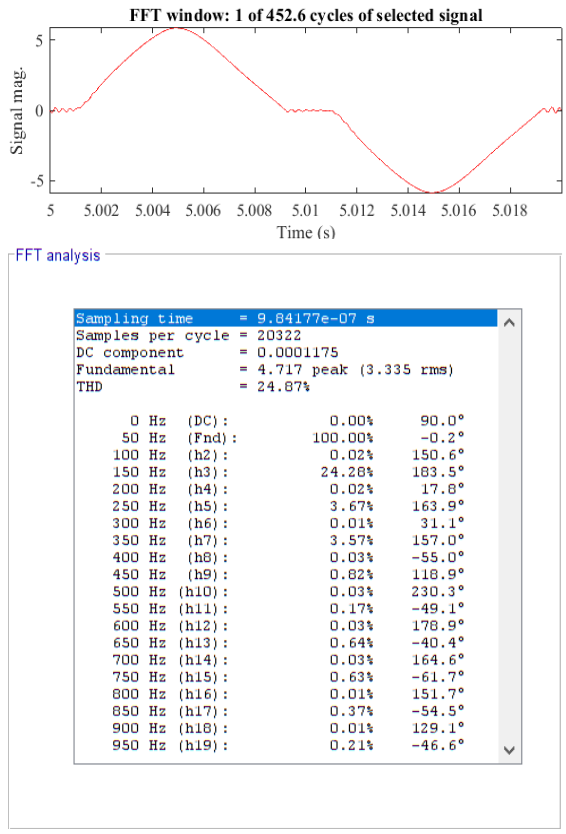

Fig. 35: FFT Analysis of Ac/DC Converter using Hysteresis current control

From the Figure 23, the Displacement Power Factor (DPF) can be identified as 1 and THD form Figure 15 can be identified as 24.87. The Power Factor can be calculated as:

$$PF = \frac{DPF}{\sqrt{1+THD^2}} \quad (45)$$

$$PF = \frac{0.99}{\sqrt{1+0.2487^2}} = 0.97 \quad (46)$$

from the Figure 15 and from Eq.12 conduction angle

$$\theta = (4.469 - 4.461) * \frac{180}{0.01} = 144° \quad (47)$$

Table 1. Performance of AC/DC Converter with Open loop and closed loop configuration

Converter	DPF	THD%	Power Factor	Voltage Across the Switch (V) and Output Voltage (V)
AC/DC Converter Without EMI Filter	0.99	73.51	0.8	50 and 46.13
AC/DC Converter With EMI Filter (open loop)	0.99	61.20	0.84	60 and 46.12
AC/DC Converter using hysteresis current controller. (closed loop)	1	24.87	0.97	51 and 48V

From the above Table 1 it is concluded that the proposed converter is giving better performance using Hysteresis current control. Hence the hardware implementation is done by using hysteresis current control.

5 Hardware Results of AC/DC Converter using Hysteresis Current Control

Figure 36 shows Hardware prototype of AC/DC converter using FPGA SPARTRAN6. This FPGA is used to generate PWM Pulses of hysteresis current mode control. Figure 37, Figure 38 and Figure 39 shows the output voltage, current and Input current and voltage waveforms of the proposed AC-DC-DC Converter in order. Figure 40 and Figure 41 shows THD using power quality analyzer and showing that 14.73%.

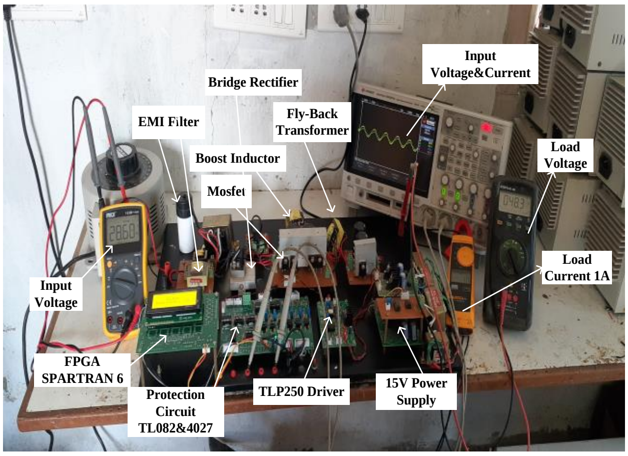

Fig. 36: Hardware prototype of AC/DC Converter using FPGA SPARTRAN 6

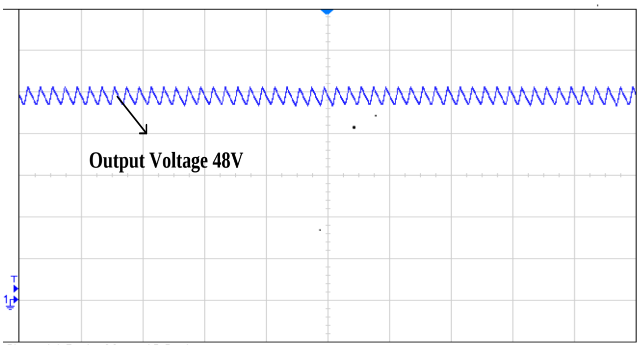

Fig. 37: Output Voltage of AC/DC Converter with Hysteresis Control. (10v/div)

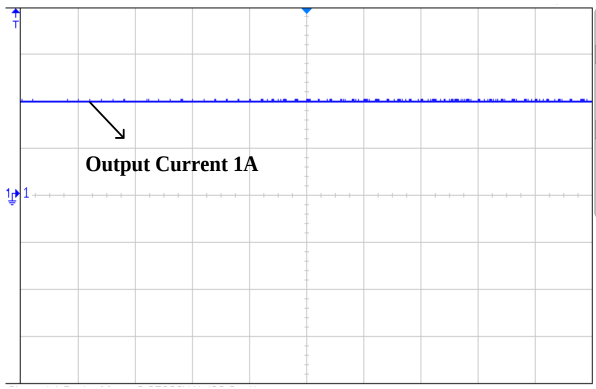

Fig. 38: Output Current of AC/DC Converter with Hysteresis Control. (0.5A/div)

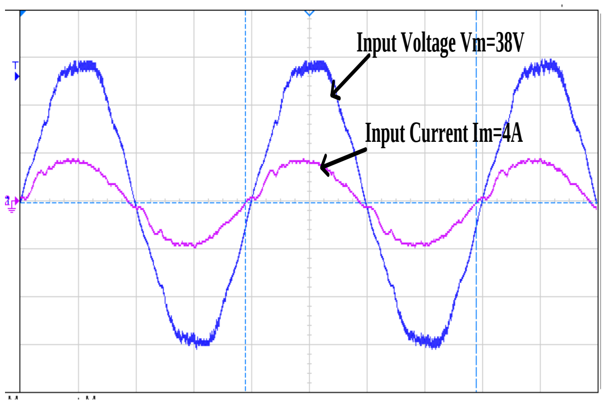

Fig. 39: Input Voltage and Input Current of AC/DC Converter with Hysteresis Control (10V/div,5A/div)

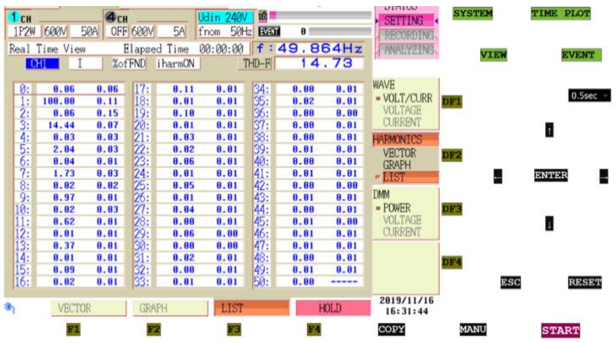

Fig. 40: Total Harmonic Distortion (THD) measured from Power Quality Analyser

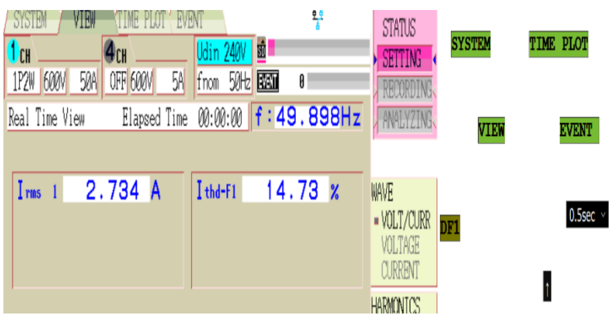

Fig. 41: Total Harmonic Distortion (THD) & Fundamental Component of Current measured from Power Quality Analyzer

6 Conclusion

In this paper low voltage AC input Boost fly back converter with series parallel combination is implemented for 48W Application. The 48W application is generally comes under Class C Application. MATLAB Simulation and Hardware implementation is done using FPGA SPARTRAN 6. By using Hysteresis current control, the converter gives better performance compare to the open loop with EMI Filter and open loop without EMI Filter. By using Hysteresis current control Power factor is 0.97 and THD is 24.73% in case of simulation and 14.73 in case of hardware implementation. The efficiency of the converter is 72%. From the FFT Analysis and power quality analyzer it is observed that third and fifth harmonics are satisfied as per IEC-1000-3-2 and EN-61000-3-2 standards.

References:

[1] Z. Dong. Nonlinear adaptive power-level control for modular high temperature gas cooled reactors. *IEEE Transactions on Nuclear Science*, 60(2), pp. 1332-1345, (2017).

[2] T. J. Liang, J. H. Lee, S. M. Chen, and L. S. Yang. Novel isolated high step-up DC–DC converter with voltage lift. *IEEE Transactions on Industrial Electronics*, 60(4), pp. 1483-1491, (2013).

[3] S. K. Changchien, T. J. Liang, J. F. Chen, L. S. Yang. Novel high step-up DC-DC converter for fuel cell energy conversion system. *IEEE Transactions on Industrial Electronics*, 57(6), pp.1483-1491, (2010).

[4] J. Wang, F. Z. Peng, J. Anderson, A. Joseph, and R. Buffenbarger. Low-cost fuel cell converter system for residential power generation. *IEEE Transactions on Power Electronics*. 19(5), pp. 1315–1322, (2004).

[5] Y. P. Hsieh, J. F. Chen, L. S. Yang, C.Y. W, and W. S. Liu. High conversion-ratio bidirectional DC-DC converter with high coupled inductor. *IEEE Transactions on Industrial Electronics*, 61(1), pp. 210-222, (2014)

[6] E. Sanchis, E. Maset, A. Ferreres, J. B. Ejea, V. Esteve, J. Jordan, J. Calvente, A. Garrigos, and J. M. Blanes. Bidirectional high-efficiency non isolated step-up battery regulator. *IEEE Transactions on Aerospace and Electronic Systems*, 47(3), pp. 2230-2239, (2011).

[7] R. J. Wai, R. Y. Duan, and K. H. Jheng. High-efficiency bidirectional dc–dc converter with high-voltage gain. *IET Power Electronics*, 5(2), pp. 173–184, (2012).

[8] Sravan kumar soma, Ravisankara Reddy Netapally, Vijaya kumar Mallapu. Low-Stress and Efficient Design of Integrated Boost Series Parallel Fly-Back Converters. *Journal Européen des Systèmes Automatisés*, 53(3), pp 393-401, (2020).

[9] Yashu Swami. Design Guidelines for Low Power Embedded Systems using Low Power Electronics. *WSEAS Transactions on Electronics*, 2023; 14:65-70, https://doi.org/10.37394/232017.2023.14.8.

[10] Djamila Cherifi, Yahia Miloud. Contribution to the Improvement of Sensorless DTC-SVM for Three-Level NPC Inverter-fed Induction Motor Drive. *WSEAS Transactions on Power Systems*, 2023; 18:436-445, https://doi.org/10.37394/232016.2023.18.43.

[11] S.L.V Sravan kumar. N R sankara Reddy, M Vijay kumar, Quasi Switched capacitor based integrated boost series parallel fly back converter for energy storage applications. *Journal of scientific and Industrial Research*. 78, pp 711-715, (2019).

[12] Katuri, R., & Gorantla, S. (2020). Modeling and analysis of hybrid controller by combining MFB with FLC implemented to ultracapacitor-based electric vehicle. *WSEAS Transactions on Power Systems*, 15, 21-29, https://doi.org/10.37394/232016.2020.15.3.

[13] Fatih M. Tuztasi, Ali Bekir Yildiz, Hasan Kelebek. Modeling and Analysis of DC-DC CUK Converter with Coupled Inductors. *WSEAS Transactions on Circuits and Systems*. 2022; 21:188-192, https://doi.org/10.37394/23201.2022.21.21.

[14] Irinel Valentin Pletea, Mariana Pletea, Dimitrie Alexa. Rectifier with Near Sinusoidal Input Currents Vector-controlled for AC Motor Drive. *WSEAS Transactions on Electronics*, 2022; 13:19-22, https://doi.org/10.37394/232017.2022.13.3.

[15] Katuri, R., & Gorantla, S. (2023). Design and comparative analysis of controllers implemented to hybrid energy storage system based solar-powered electric vehicle. *IETE Journal of Research*, 69(7), 4566-4588.

[16] Hayat El Aissaoui, Abdelghani El Ougli, Belkassem Tidhaf. MPPT Using PSO Technique Comparing to Fuzzy Logic and P&O algorithms for Wind Energy Conversion System. *WSEAS Transactions on Systems and Control*, 2022; 17:305-313, https://doi.org/10.37394/232017.2022.13.3.

[17] H. Wu, Y. Jia, F. Yang, L. Zhu and Y. Xing, "Two-Stage Isolated Bidirectional DC–AC Converters with Three-Port Converters and Two DC Buses," in *IEEE Journal of Emerging and Selected Topics in Power Electronics*, vol. 8, no. 4, pp. 4428-4439, Dec. 2020.

[18] I. Alhurayyis, A. Elkhateb and J. Morrow, "Isolated and Nonisolated DC-to-DC Converters for Medium-Voltage DC Networks: A Review," in *IEEE Journal of Emerging and Selected Topics in Power Electronics*, vol. 9, no. 6, pp. 7486-7500, Dec. 2021

[19] M. Ashraf, Y. Nazih, F. Alsokhiry, K. H. Ahmed, A. S. Abdel-Khalik and Y. Al-Turki, "A New Hybrid Dual Active Bridge Modular Multilevel Based DC–DC Converter for HVDC Networks," in *IEEE Access*, vol. 9, pp. 62055-62073, 2021.

[20] I. N. Jiya, A. Salem, H. Van Khang and R. Pomarnacki, "Integrated Multiport DC-DC and Multilevel Converters for Multiple Renewable Energy Source Integration," in *IEEE Access*, vol. 11, pp. 132483-132495, 2023.

Contribution of Individual Authors to the Creation of a Scientific Article (Ghostwriting Policy)

The authors equally contributed in the present research, at all stages from the formulation of the problem to the final findings and solution.

Sources of Funding for Research Presented in a Scientific Article or Scientific Article Itself

No funding was received for conducting this study.

Conflict of Interest

The authors have no conflicts of interest to declare.